Desorption and Rearrangement Kinetics of Carbon Monoxide on a PEM Fuel Cell Electrode

Vijay A. Sethuraman[*, 1], Balasubramanian Lakshmanan[*, 2], and John W. Weidner[*, z]

Center for Electrochemical Engineering
Department of Chemical Engineering
University of South Carolina, Columbia, SC 29208, USA

Submitted as a technical paper to
Professor Daniel A. Scherson, Editor
Journal of the Electrochemical Society
(A Publication of the Electrochemical Society)
65 South Main Street, Pennington, NJ 08534-2839, USA

Submission date: April 11, 2008

[z] – Corresponding author: Phone: (803) 777-3207; Fax: (803) 777-8265
E-mail: weidner@engr.sc.edu (J. W. Weidner)
[1] – Present address: Environmental Energy Technology Division, MS 70-R0108B, Lawrence Berkeley National Laboratory, Berkeley, CA 94720
[2] – Present address: General Motors Fuel Cell Activities, 10 Carriage Street, Honeoye Falls, NY 14472
[*] - Electrochemical Society Active Member

Abstract

A procedure to measure the kinetics of carbon monoxide (CO) desorption from, and simultaneous rearrangement on, supported platinum (Pt on Vulcan XC-72R) fuel cell electrode is reported. The surface coverage of CO on Pt electrode was measured from the anodic peaks in the CO stripping voltammogram. Two distinct CO oxidation peaks observed in the voltammogram due to the oxidation of two distinct ad-species, namely weakly adsorbed CO (CO_{ad}^{I}) and strongly adsorbed CO (CO_{ad}^{II}), were baseline corrected and deconvoluted using a bimodal Gaussian distribution. This data was fit using a kinetic model to extract desorption and rearrangement rate constants as a function of temperature. Saturation surface coverage of CO_{ad}^{I} decreased with increasing temperature, while the opposite was true for CO_{ad}^{II}. Rearrangement from CO_{ad}^{II} to CO_{ad}^{I} was faster than the desorption rate of either of the CO molecules. The desorption rate of CO_{ad}^{II} was at least an order of magnitude lower than that of CO_{ad}^{I} molecules at all temperatures studied. The activation energies for desorption of CO_{ad}^{I} and CO_{ad}^{II} were estimated to be 24.08 and 27.99 kJ/mole, respectively. The activation energy for rearrangement from CO_{ad}^{I} to CO_{ad}^{II} was 35.23 kJ/mol and that from CO_{ad}^{II} to CO_{ad}^{I} was 27.55 kJ/mol.

Introduction

The electro-oxidation of carbon monoxide (CO) on single crystal and polycrystalline Pt electrodes is of considerable interest because of CO poisoning in PEM fuel cells operating on hydrogen derived from hydrocarbons. Gilman[1,2] first showed the existence of two anodic peaks in CO stripping voltammograms and it is now generally agreed that when CO is adsorbed on Pt under steady-state conditions and at potentials in the neighborhood of hydrogen reversible potential, two anodic peaks appear in the stripping voltammogram.[3-8] The spectroscopic nature of CO adsorption on Pt was studied in the early 1950s by Eischens and Pliskin[9] using infrared techniques, where they showed evidence for two types of CO structures adsorbed on Pt supported on cabosil and alumina. The spectroscopic nature of the adsorbed CO has been well studied since then using a variety of techniques and shown to be dependent on the surface coverage and the potential of the electrode at which CO was adsorbed. [10-12] Surface coverage of one of the CO species was shown to be higher than the other in surfaces adsorbed at higher potentials (>0.5 V vs. SHE).[10] Currently, no clear correlation exists in the literature between nature of CO adsorption and their oxidation potentials.[13]

Markovic et al. studied the electro-oxidation of CO on Pt(111) in acid solutions at room temperature using voltammetry on a rotating disc electrode (RDE) in conjunction with *in situ* surface X-ray diffraction (XRD) measurements. They reported the presence of weakly (CO_{ad}^{I}) and strongly (CO_{ad}^{II}) bound CO species and that the former forms at saturation coverage and assumes a p(2x2) structure containing three CO molecules per unit cell (0.75 CO/Pt) and its oxidative removal was accompanied by simultaneous relaxation of CO adlayer with the remaining CO_{ad}^{II} (0.6 CO/Pt) assuming a new bonding

state.[14] The electro-oxidation of CO_{ad}^{I} and CO_{ad}^{II} were respectively attributed to the first and second peaks observed in the CO stripping voltammograms. In this work, we use these CO/Pt values to calculate the number of Pt sites with weakly and strongly adsorbed CO molecules based on the respective coulombic charges obtained from the CO stripping voltammograms.

The objective of this work was to quantify the desorption and rearrangement kinetics of CO_{ad}^{I} and CO_{ad}^{II} as a function of temperature relevant to PEM fuel cell operation. This was accomplished by first measuring the surface coverages of CO_{ad}^{I} and CO_{ad}^{II} after saturation with CO in the gas phase. The decline in these surface coverages due to desorption and rearrangement, once CO was replaced by N_2 in the gas phase, were then measured as a function of desorption time. The relevant rate constants were then estimated by fitting this data to a kinetic model. The respective activation energies were estimated by repeating these procedures at different temperatures.

Experimental

Fuel cell electrode fabrication – Pt catalyst ink with 75% catalyst and 25% Nafion® (dry solids content) was prepared with commercially available 40 wt% Pt on Vulcan XC-72R E-TEK® catalyst (PEMEAS Fuel Cell Technologies, Somerset, NJ). Nafion® in the form of perfluorosulfonic acid-PTFE copolymer (5% w/w solution, Alfa Aesar, Ward Hill, MA) was used. The catalyst ink was sprayed on to gas diffusion layers (ELAT® GDL, 10 cm^2 active area, PEMEAS Fuel Cell Technologies, Somerset, NJ) with N_2 brush (Paasche Airbrush Company, Chicago, IL), air dried for thirty minutes and then dried under vacuum (381 mm Hg) at 110 °C for 10 minutes to evaporate any remaining

solvent. This process was repeated until a catalyst loading of 0.5 mg Pt/cm^2 was achieved. Two such catalyst coated GDLs were then bonded to either side of a pretreated Nafion® 112 membrane (Alfa Aesar, Ward Hill, MA) by hot pressing (140 °C, 2 minutes, for two minutes at 3450 kPa to make a membrane electrode assembly (MEA). The MEA was then assembled into a fuel cell with single channel serpentine flow field plates (Fuel Cell Technologies Inc., Albuquerque, NM). The cell was operated at 0.4 A/cm^2 for 8 hours at 70 °C and 101.325 kPa with a flow of 0.12 standard liters per minute (SLM) H_2 and 0.36 SLM air on the anode and cathode sides, respectively. Polarization (V-I) curves were recorded and compared to a baseline V-I curve to confirm that the fuel cell was working properly. All pure gases (except for industrial grade air) used in the experiments were obtained from Air Products and were certified ultra high purity (UHP)

CO coverage – After the fuel cell conditioning process, the cathode gas was switched to H_2 at 0.05 SLM, which acted as counter and reference electrode (i.e., dynamic hydrogen electrode, DHE). All potentials reported here refer to this electrode. The anode gas was switched to N_2 at 0.1 SLM. After allowing the N_2 to purge through the fuel cell channels, flow was switched to 476 ppm CO in N_2 (hereafter referred to as CO/N_2) at 0.10 SLM for 300 seconds. This exposure time was approximately twice the residence time of the gas channels and ensured complete exposure of the Pt to CO. Nitrogen flow was restored after this exposure. An exposure time of 300 ± 100 seconds did not affect the results shown here and that electrode reaches a steady state condition (i.e., the surface coverage did not change with time; see discussion for Figure 3). After a wait period of 30 seconds, the cell was held at a constant potential of 50 mV for 25 seconds followed by a CV at the rate of 20 mV s^{-1} from 50 to 1150 mV and back to 50

mV. Experiments were conducted using a M263A potentiostat/galvanostat (Princeton Applied Research Inc., Oak Rindge, TN) and ECHEM® software made by EG&G. The area under the CO oxidation peak, Q_{CO}, in the potential window 600 – 850 mV relative to the background current was used to calculate the amount of CO oxidized, which was taken to be the amount of CO adsorbed. The area under H_2 desorption peak, Q_H, in the potential window 50 -350 mV corrected for the background was also measured. The experiment was repeated for various durations of CO/N_2 exposure. Between each experiment, another CV was performed on the electrode and the resulting CV overlapped with the background, confirming that all adsorbed CO was oxidized in the first cycle.

Figure 1 shows a representative CV before and after CO adsorption. The dotted and the solid lines correspond to a clean and CO adsorbed electrode, respectively. The broad peak between 50-400 mV and the two distinct peaks between 600-1000 mV correspond to hydrogen ($\text{Pt-H} \rightarrow \text{Pt} + \text{H}^+ + \text{e}^-$) and CO oxidation ($\text{Pt}_x\text{-CO} + \text{Pt}_x\text{-H}_2\text{O} \rightarrow 2x\text{Pt} + \text{CO}_2 + 2\text{H}^+ + 2\text{e}^-$; x=h,k) with their electrochemical areas represented by Q_H and Q_{CO}, respectively. The areas under hydrogen and CO peaks were 598 mC and 880 mC, respectively. The charge under the voltammetric peaks for hydrogen desorption, corrected for double layer charging was assumed to correspond to one hydrogen atom on each Pt atom on the surface. Oxidation current from CO covered electrode in the 50-400 mV potential window was used as the baseline for estimating the coulombic area of hydrogen desorption. Current from a clean electrode in the 500-800 mV potential window was used as the baseline for estimating the coulombic area corresponding to CO oxidation.

CO desorption – To extract the rate of CO desorption from the Pt/C electrodes the amount of CO remaining on the electrode was determined as a function of desorption time. The electrode was exposed to CO/N_2 for 300 seconds after which the flow on the anode side was switched to N_2. A CV was conducted after waiting for a specific duration called as desorption time. The cell was at open circuit (*ca.* 80 mV vs. DHE) during CO exposure and desorption steps. The area under the CO oxidation peaks in the resulting CVs was estimated as outlined below. The adsorption, desorption and voltammetry steps were repeated for various desorption times and temperatures.

The CVs obtained on a CO covered electrode were baseline corrected and the peaks were deconvoluted with a bimodal Gaussian distribution using commercially available software (Tablecurve2D®, Systat® Software Inc., San Jose, CA). The general form of bimodal Gaussian distribution used for this case is given as,

$$I = a\,e^{-\left(\frac{V-b}{c}\right)^2} + d\,e^{-\left(\frac{V-e}{f}\right)^2} \qquad 1$$

The process for deconvoluting the two peaks involved the following steps: baseline corrected data was imported into the Tablecurve2D®, data was filtered to represent the voltage window of interest, the filtered data was fit to a general form of a bimodal Gaussian distribution and the fitting parameters (a, b, …, f) were iterated to maximize the R^2 and F-value. The result of this process for the CV shown in Figure 1 is given in Figure 2. The resulting fit for all deconvolutions had an R^2 greater than 0.98 and the deconvolution parameters were estimated with a 95% or higher confidence interval. The deconvolution in Figure 2 shows two overlapping peaks with a peak height of about 100 mA and 75 mA for the first and second peaks, respectively. The miniscule shoulder observed on the left side of the first peak was routinely observed on most of the CVs

conducted at lower temperatures (< 40 ºC). This could be due to a third kind of adsorption, i.e., CO on a hollow site. This shoulder or the 'third peak' was treated as oxidation of a weakly bound CO molecule in this work. The sum of these two peaks was fit to the experimental data with an R^2 greater than 0.99.

Model development. - The first peak occurring at a lower potential was assigned to the oxidation of weakly adsorbed CO molecules (CO_{ad}^{I}) and the area under this peak was designated as Q_{CO}^{I}. Similarly, the second peak occurring at a higher potential was assigned to the oxidation of strongly adsorbed CO molecules (CO_{ad}^{II}) and the area under this peak was designated as Q_{CO}^{II}. The fraction of Pt sites covered by CO_{ad}^{I} and CO_{ad}^{II} were expressed respectively as,

$$\theta_{CO}^{I} = \frac{h_I Q_{CO}^{I}}{\left[h_I Q_{CO}^{I} + h_{II} Q_{CO}^{II} \right]_{max}} \qquad 2$$

$$\theta_{CO}^{II} = \frac{h_{II} Q_{CO}^{II}}{\left[h_I Q_{CO}^{I} + h_{II} Q_{CO}^{II} \right]_{max}} \qquad 3$$

where, $\left[h_I Q_{CO}^{I} + h_{II} Q_{CO}^{II} \right]_{max}$ was the maximum area under the CO peaks. The parameters h_I and h_{II} correspond to the reciprocal of number of CO molecules adsorbed per Pt site (CO/Pt) for CO_{ad}^{I} and CO_{ad}^{II}, respectively. Values of $1/h_I$=0.75 and $1/h_{II}$ = 0.6 based on data from Markovic *et al.*[14] were used. The fraction of Pt sites covered by CO molecules was the sum of fractional coverage of CO_{ad}^{I} and CO_{ad}^{II} given by equation [4].

$$\theta_{CO} = \theta_{CO}^{I} + \theta_{CO}^{II} \qquad 4$$

The fraction of the vacant sites, θ_v was obtained from the site balance.

$$\theta_v = 1 - \theta_{CO} = 1 - \theta_{CO}^{I} - \theta_{CO}^{II} \qquad 5$$

Good agreement on site balance based on Q_H and Q_{CO} was reached by using CO/Pt values reported by Markovic et al. (i.e., 0.75 CO/Pt for Q_{CO}^{I} and 0.6 CO/Pt for Q_{CO}^{II}) along with the fractional coverage obtained from the deconvolution results. The value of $\left[h_I Q_{CO}^{I} + h_{II} Q_{CO}^{II}\right]_{max}$ was within 5% of $2Q_H^0\big|_{max}$ indicating slightly less than a monolayer coverage of CO on the Pt/C electrodes at maximum coverage (see Figure 1).

CO adsorption, desorption and rearrangement proceed through the following reaction scheme, consistent with previous observation of dual modes of adsorption.

$$CO + Pt \underset{k_{-1}}{\overset{k_1}{\rightleftarrows}} CO_{ad}^{I} \qquad 6$$

$$k_{-3} \uparrow\downarrow k_3 \qquad 7$$

$$CO + Pt \underset{k_{-2}}{\overset{k_2}{\rightleftarrows}} CO_{ad}^{II} \qquad 8$$

Reactions [6] and [8] correspond to the adsorption and desorption of CO_{ad}^{I} and CO_{ad}^{II}, respectively. Note that the Pt sites in these reactions are not meant to be stoichiometrically balanced. Reaction [**7**] corresponds to the rearrangement between the weakly and strongly bound CO molecules. Spectroscopic proof of surface equilibrium between CO_{ad}^{II} and CO_{ad}^{I} has been reported before.[15] The following general assumptions were made for developing the kinetic model:

(1) All Pt sites were assumed equivalent

(2) Pt sites did not change during the experiments. Though the applied potential during CV sweeps routinely exceeded the equilibrium potential for Pt dissolution (~1.0V vs. DHE), Pt sites were assumed not to dissolve, migrate or ripen for the duration of the experiment. This is a valid assumption because of the duration of the applied potential, which was of the order of few minutes as opposed to the time constant for Pt dissolution and migration, which was shown to be at least two orders of magnitude higher

(3) Isothermal conditions exist and

(4) The reactions were assumed first order with respect to reactants (i.e., CO and Pt sites)

The material balance for the surface coverage of Pt sites during desorption and rearrangement of CO^{I}_{ad} and CO^{II}_{ad} are given by equations [9] and [10], respectively,

$$\frac{d\theta^{I}_{CO}}{dt} = -k_{-1}\theta^{I}_{CO} - \left(\frac{1}{h_{II}} - \frac{1}{h_{I}}\right)k_{3}\theta^{I}_{CO}\theta_{v} + k_{-3}\theta^{II}_{CO} \qquad \mathbf{9}$$

$$\frac{d\theta^{II}_{CO}}{dt} = -k_{-2}\theta^{II}_{CO} + \left(\frac{1}{h_{II}} - \frac{1}{h_{I}}\right)k_{3}\theta^{I}_{CO}\theta_{v} - k_{3}\theta^{II}_{CO} \qquad \mathbf{10}$$

Desorption and the rearrangement rate constants were estimated first using data obtained from the desorption experiments.

Parameter estimation. – Equations [9] and [10] were then solved simultaneously with k_{-1}, k_{-2}, k_3, and k_{-3} as parameters using the known initial surface coverages. The Levenberg-Marquardt method[16], a non-linear parameter estimation procedure, was used to estimate these parameters. Numeric Dsolve® subroutines in Maple® (Maplesoft®, Waterloo, ON, Canada) were used to solve the differential equations. The activation energies were estimated from data obtained by repeating the experiments at different temperatures and by fitting the estimated rate constants to the form,

$$k_n = k_n^0 \exp\left(\frac{-E_a}{RT}\right) \qquad 11$$

where E_a was the corresponding activation energy.

Results and Discussion

Figure 3 shows CVs obtained on a Pt electrode with N_2 in the gas phase after exposure to 476 ppm CO in N_2 for different exposure times and for a clean Pt electrode. The amount of CO adsorbed was equal to the amount fed for all exposure times below 300 seconds. The CO adsorption on Pt in this system was transport limited (i.e., limited by the amount fed) and an implication of this was that the adsorption rate constants (k_1 and k_2) could not be reliably measured. The amount of CO adsorbed and the nature of oxidation peaks did not change for exposure times greater than 300 seconds. For example, the CVs corresponding to exposure times of 300 and 450 seconds shown in Figure 3 overlap.

Figure 4 shows some of the CVs from a set of CVs obtained on Pt electrode after exposure to 476 ppm CO in N_2 at 0.10 SLM for 300 seconds as a function of temperature. With the increase in temperature, the CO peak shifts towards lower potential. For example, the potential corresponding to the peak current decreased from 609 mV to 559 mV when the temperature increased from 70 to 90 °C. Conversely, the peak current increased from 770 mA to 970 mA for the same increase in temperature mentioned above. Both phenomena are well documented in the literature. However, the change in the peak structure with increase in temperature, as seen in Figure 4, had never been discussed before in the literature. This indicates that the increase in the electro-oxidation rate constants with temperature could be different for CO_{ad}^{I} and CO_{ad}^{II}. Figure 5 shows

the surface coverages of CO^{I}_{ad} and CO^{II}_{ad} obtained from the set of CVs shown in Figure 4. These represent the initial CO coverage for the fit to the rate expressions given by 9 and 10. The sum of these coverages (equation 4) was 1±0.05. Therefore, in the presence of CO in the gas phase no vacant Pt sites exist. Again, an implication of this would was the adsorption rate constants cannot be measured using 9 and 10. However, the ratio of k_1 to k_2 or vice versa (relative adsorption rates) can be estimated using Q^{I}_{CO} and Q^{II}_{CO} measured from CVs shown in Figure 3.

Figure 6 shows CVs on Pt electrode after various desorption times at 95 °C. The peak current and the CO oxidation area decrease with the increase in desorption time confirming considerable desorption of CO molecules in the given period. For example, the peak current decreased from 555 mA to 447 mA and the peak potential decreased from 542 mV to 534 mV when the desorption time was increased from 5 to 15 minutes, respectively. The decrease in peak potential with increasing desorption time can be attributed to the lower surface coverage which enables the formation of oxidative OH species at lower potentials and is consistent with similar observation on single crystal Pt electrodes by Cuoto *et al*.[7] On close inspection, a shoulder growth occurring at potentials lower that the main peak can be seen even for short duration (less than 300 s). Even though there was considerable reduction in the area under the CO peak, there was no corresponding increase in the area under the hydrogen oxidation region suggesting that not much free sites are formed. This could only be explained, if CO^{II}_{ad} were rearranging to CO^{I}_{ad} thereby leading to minimal change in free sites even after considerable decrease in CO area. Therefore, the shoulder occurring at lower potentials was attributed to the increase in the surface coverage of CO^{I}_{ad} .

Figure 7 shows the overall surface coverage of CO as a function of desorption time at 95 ºC. The data points were obtained from the CVs shown in Figure 6 and the solid line correspond to the least squares fit. The parameter estimation procedure involved solving for the desorption and rearrangement rate constants using equations [9] and [10] together with their initial conditions. The model predictions using the fitted parameters are shown in Figure 8. The CO_{ad}^{I} (●) and CO_{ad}^{II} (○) surface coverages are indicated as a function of desorption time. The predicted surface coverages for CO_{ad}^{I} and CO_{ad}^{II} compare very well with the individual areas thus validating the parameter estimation procedure. It must be noted that the confidence for the re-arrangement rate constants was relatively low due to fewer number of data points in the medium range of desorption times.

The parameter estimation routine was repeated for experimental data obtained at temperatures between 50 and 95 ºC and the kinetic rate constants were determined. Analysis was done in this temperature range because CO desorption was too slow at lower temperatures (i.e., < 50 ºC). Also, at temperatures higher than 100 ºC, the deconvoluting the CVs with good confidence tends to be difficult. Figure 9 shows the Arrhenius plot of the parameters from 50 to 95 ºC. The symbols correspond to the different kinetic rate constants as indicated by the legend. The rate constants (symbols) in Figure 9 was fit to equation 11, resulting in,

$$k_{-1} = 0.3304 \exp\left(-\frac{24082}{RT}\right)$$
$$k_{-2} = 0.387 \exp\left(-\frac{27995}{RT}\right)$$
$$k_{3} = 8.9484 \exp\left(-\frac{35229}{RT}\right)$$
$$k_{-3} = 1.8686 \exp\left(-\frac{27550}{RT}\right) \qquad \textbf{12}$$

The activation energy for desorption of CO_{ad}^{I} and CO_{ad}^{II} were 24.08 and 27.99 kJ/mole, respectively. The activation energy for rearrangement from CO_{ad}^{I} to CO_{ad}^{II} was 35.23 kJ/mol and that from CO_{ad}^{II} to CO_{ad}^{I} was 27.55 kJ/mol. The lower activation energy for desorption of CO_{ad}^{I} than CO_{ad}^{II} is consistent with the observation by Markovic et al. Further, this is also consistent with the spectroscopic data[9] in that CO_{ad}^{I} appears at a lower wave number (indicating weaker adsorption) than CO_{ad}^{II} in the infrared spectrum.

Conclusions

The distribution of CO_{ad}^{I} and CO_{ad}^{II} adsorbed at open circuit on a PEM fuel cell electrode was characterized using cyclic voltammetry. The surface coverage of CO_{ad}^{I} was high at low temperatures and decreased with increasing temperature, while the opposite was true for CO_{ad}^{II}. Desorption and rearrangement rate constants for CO_{ad}^{I} and CO_{ad}^{II} were determined as a function of temperature. CO desorption was controlled by the parallel desorption from CO_{ad}^{I} and CO_{ad}^{II}; and simultaneous rearrangement between them. Rearrangement from CO_{ad}^{II} to CO_{ad}^{I} was faster than either of the desorption rates over the entire range of temperature studied. The desorption rate of CO_{ad}^{II} was at least an

order of magnitude lower than that of CO_{ad}^{I}. The activation energies for desorption of CO_{ad}^{I} and CO_{ad}^{II} were estimated to be 24.08 and 27.99 kJ/mole, respectively. The activation energy for rearrangement from CO_{ad}^{I} to CO_{ad}^{II} was 35.23 kJ/mol and that from CO_{ad}^{II} to CO_{ad}^{I} was 27.55 kJ/mol. The accuracy and confidence on these estimated values can be improved by repeating the experiments and collecting more data at the intermediate desorption time range. Further estimation of electro-oxidation rate constants and the application of these constants towards designing an electrochemical CO filter[17] are currently ongoing in our laboratory.

Acknowledgement

The authors acknowledge the support from the National Reconnaissance Office for *Hybrid Advanced Power Sources* under grant # NRO-00-C-1034 and the National Science Foundation Industry/University Co-operative Research Center for Fuel Cells under award # NSF-03-24260.

List of Figures

Figure 1: (Color online) CV obtained on a 40% Pt supported on XC-72R Nafion composite electrode after exposure to 476 ppm CO in N_2 for 300 seconds at 25 °C and 101.325 kPa. Q_H and Q_{CO} correspond to the amount of H_2 and CO oxidized, respectively. The dotted and the solid lines correspond to CVs from a clean and a CO covered (steady state coverage) electrode, respectively.

Figure 2: (Color online) Baseline corrected CO oxidation peaks (from Figure 1) deconvoluted using bimodal Gaussian distribution (equation 1) shown along with the sum of two peaks. The lines (dot, dot-dash, and solid line) correspond to peaks I, II and I+II, respectively. The following parameters were used for this fit: a = 100.13, b = 735.42, c = 45.28, d = 74.75, e = 820.86 and f = 49.4

Figure 3: (Color online) Cyclic voltammograms on Pt composite electrode with N_2 in gas phase after exposure to 476 ppm CO in N_2 at a flow rate of 0.10 SLM for various exposure times (shown in the legend); and for a clean Pt composite electrode (---). The experiments were conducted at 25 °C and 101.325 kPa.

Figure 4: (Color online) CVs obtained on a Pt composite electrode after exposure to 476 ppm CO in N_2 for 300 s. The experiments were conducted at 101.325 kPa and different temperatures as indicated in the legend.

Figure 5: (Color online) Experimentally measured surface coverages of CO_{ad}^{I} (-●-) and CO_{ad}^{II} (-○-) as a function of temperature. These data points were obtained by deconvoluting the CVs from the dataset shown in Figure 4 and using the resulting

coulombic charges in equations 2 and 3. The sum of these two coverages (-■-) was 1±0.05.

Figure 6: (Color online) CVs on a Pt composite electrode under N_2 flow after three sample desorption times. The electrodes were initially exposed to 476 ppm CO in N_2 for 300 s at 95 °C and 101.325 kPa.

Figure 7: (Color online) Total surface coverage of CO as a function of desorption time at 95 °C and 101.325 kPa. The data (●) was fit (solid line) to the sum of equations 9 and 10.

Figure 8: (Color online) Surface coverages of CO^{I}_{ad} (●) and CO^{II}_{ad} (○) molecules measured at 95 °C and 101.325 kPa were compared to model predictions.

Figure 9: (Color online) Arrhenius plots for desorption (k_{-1}, k_{-2}) and re-arrangement (k_3, k_{-3}) rate constants in the temperature range 50 to 95 °C. The symbols correspond to the different kinetic constants indicated by the legend. The Arrhenius expressions for each of these rate constants are given in equation 12.

List of symbols

a, b, ..., f	parameters in the bimodal Gaussian distribution function
CO_{ad}^{I}	CO species contributing to the first anodic peak
CO_{ad}^{II}	CO species contributing to the second anodic peak
E_a	activation energy, J mol^{-1}
h_I	number of Pt sites per CO molecule for CO_{ad}^{I} ,1.34
h_{II}	number of Pt sites per CO molecule for CO_{ad}^{II} , 1.67
I	current, mA
k_1	adsorption rate constant for CO_{ad}^{I} , cm^3 mol^{-1} s^{-1}
k_{-1}	desorption rate constant for CO_{ad}^{I} , s^{-1}
k_2	adsorption rate constant for CO_{ad}^{II} , cm^3 mol^{-1} s^{-1}
k_{-2}	desorption rate constant for CO_{ad}^{II} , s^{-1}
k_3	forward (from CO_{ad}^{I} to CO_{ad}^{II}) rearrangement rate constant, s^{-1}
k_{-3}	backward (from CO_{ad}^{II} to CO_{ad}^{I}) rearrangement rate constant, s^{-1}
Q_{CO}^{I}	columbic charge corresponding to the oxidation of CO_{ad}^{I} , C
Q_{CO}^{II}	columbic charge corresponding to the oxidation of CO_{ad}^{II} , C
Q_{CO}	total columbic charge corresponding to the CO oxidation, C
Q_H	total columbic charge corresponding to H_2 oxidation, C
R	universal gas constant, 8.314 J mol^{-1} K^{-1}
T	temperature, K

V	potential, mV vs. DHE

Greek

θ_{CO}^{I}	surface coverage of CO_{ad}^{I}
θ_{CO}^{II}	surface coverage of CO_{ad}^{II}
θ_{v}	surface coverage of vacant sites

superscripts

I	pertaining to weakly bound or peak I
II	pertaining to strongly bound or peak II

subscripts

ad	adsorbed
CO	carbon monoxide
H	hydrogen
v	vacant sites

Figures

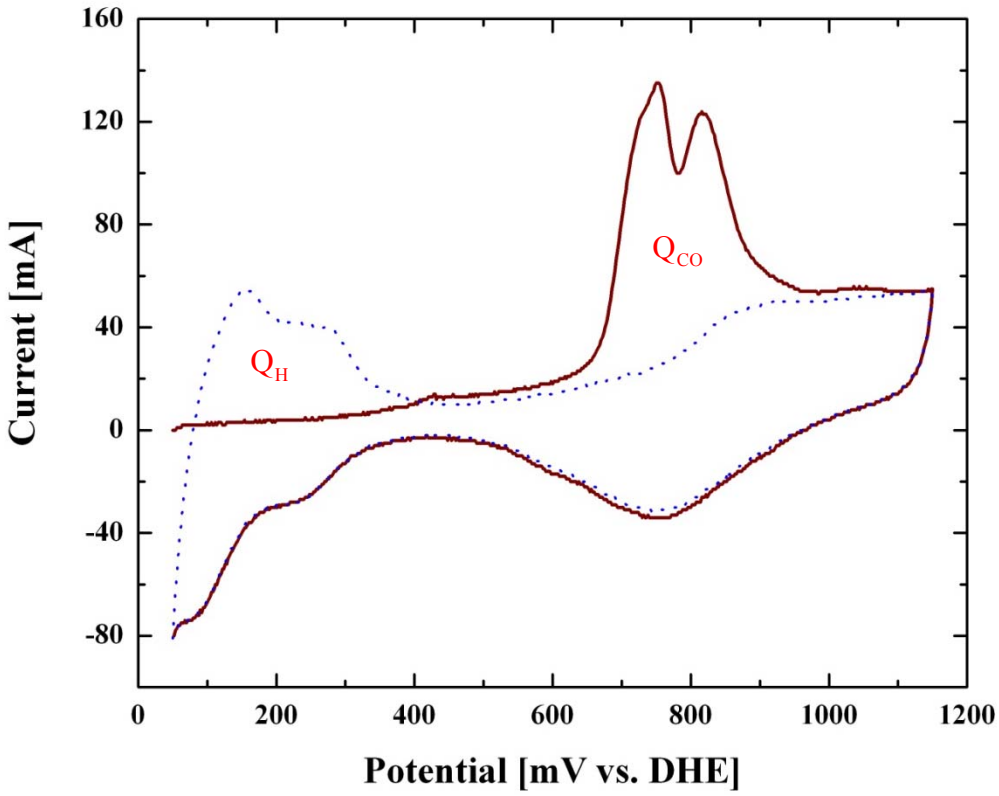

Figure 1: (Color online) CV obtained on a 40% Pt supported on XC-72R Nafion composite electrode after exposure to 476 ppm CO in N_2 for 300 seconds at 25 °C and 101.325 kPa. Q_H and Q_{CO} correspond to the amount of H_2 and CO oxidized, respectively. The dotted and the solid lines correspond to CVs from a clean and a CO covered (steady state coverage) electrode, respectively.

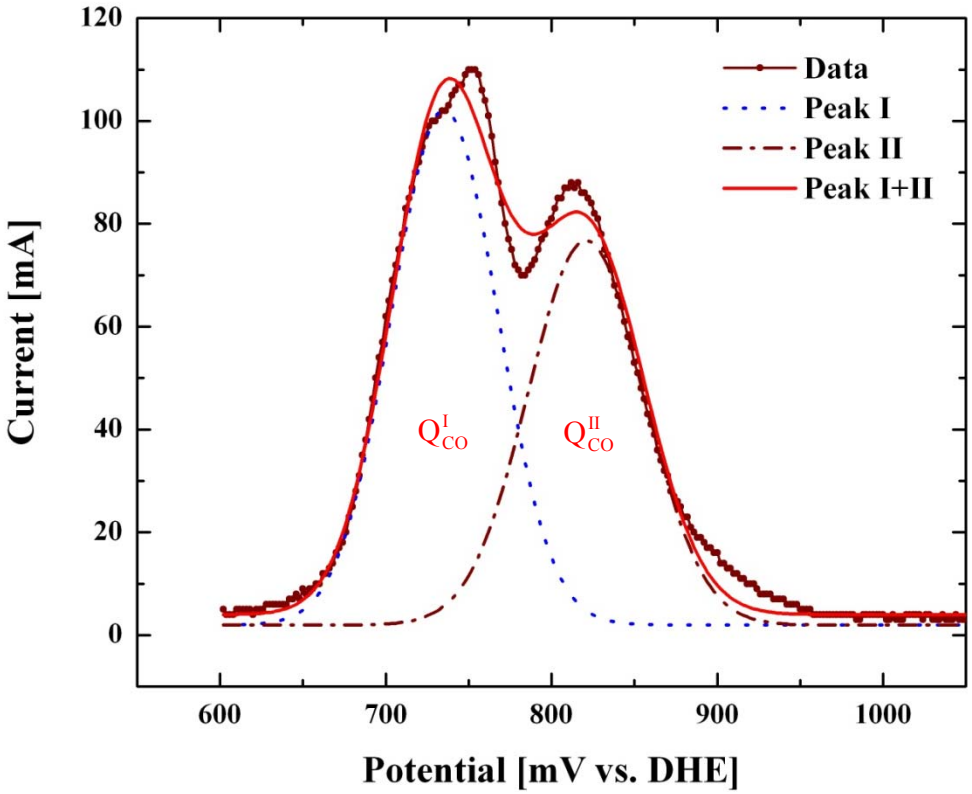

Figure 2: (Color online) Baseline corrected CO oxidation peaks (from Figure 1) deconvoluted using bimodal Gaussian distribution (equation 1) shown along with the sum of two peaks. The lines (dot, dot-dash, and solid line) correspond to peaks I, II and I+II, respectively. The following parameters were used for this fit: a = 100.13, b = 735.42, c = 45.28, d = 74.75, e = 820.86 and f = 49.4

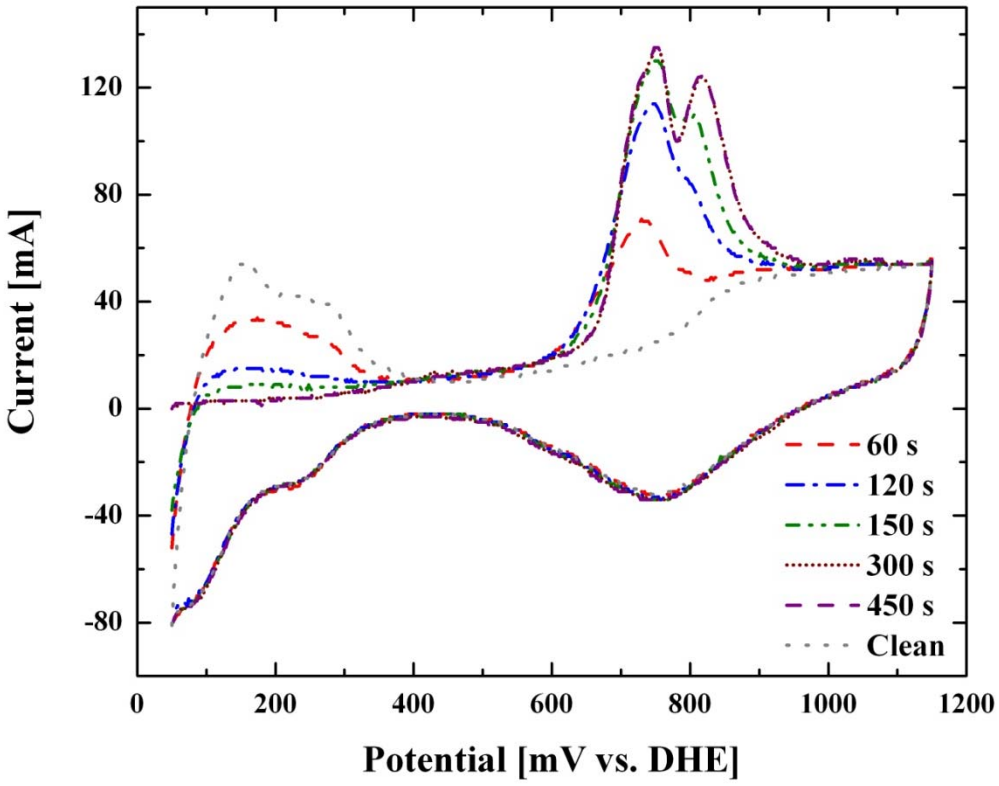

Figure 3: (Color online) Cyclic voltammograms on Pt composite electrode with N_2 in gas phase after exposure to 476 ppm CO in N_2 at a flow rate of 0.10 SLM for various exposure times (shown in the legend); and for a clean Pt composite electrode (---). The experiments were conducted at 25 °C and 101.325 kPa.

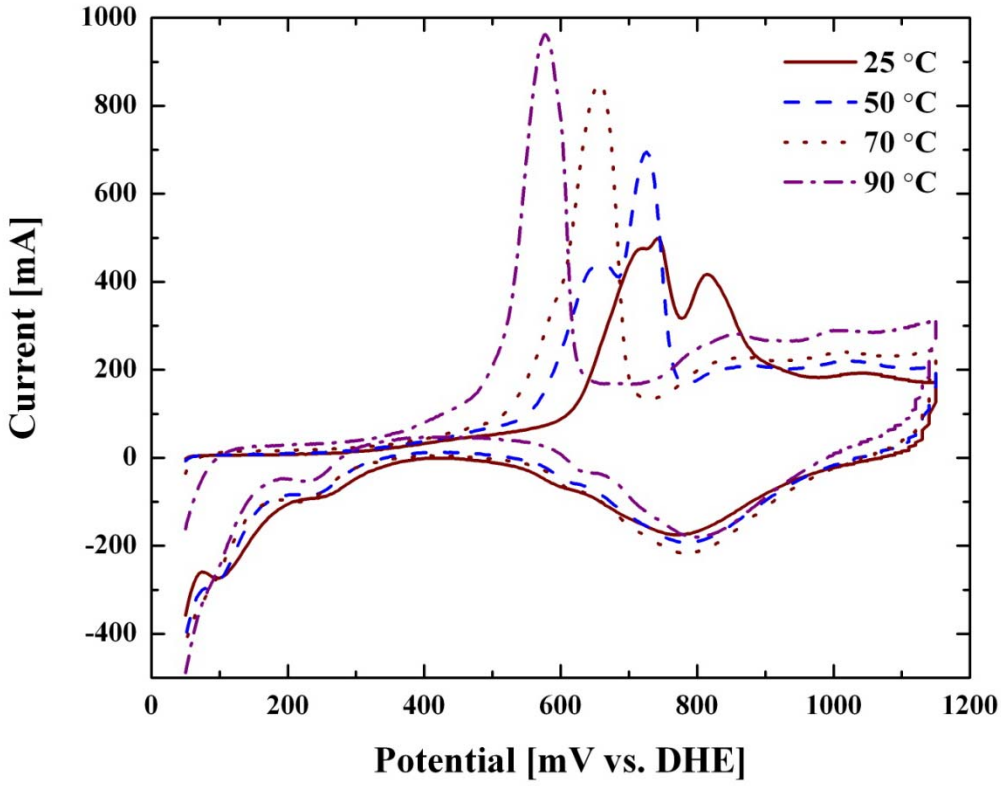

Figure 4: (Color online) CVs obtained on a Pt composite electrode after exposure to 476 ppm CO in N_2 for 300 s. The experiments were conducted at 101.325 kPa and different temperatures as indicated in the legend.

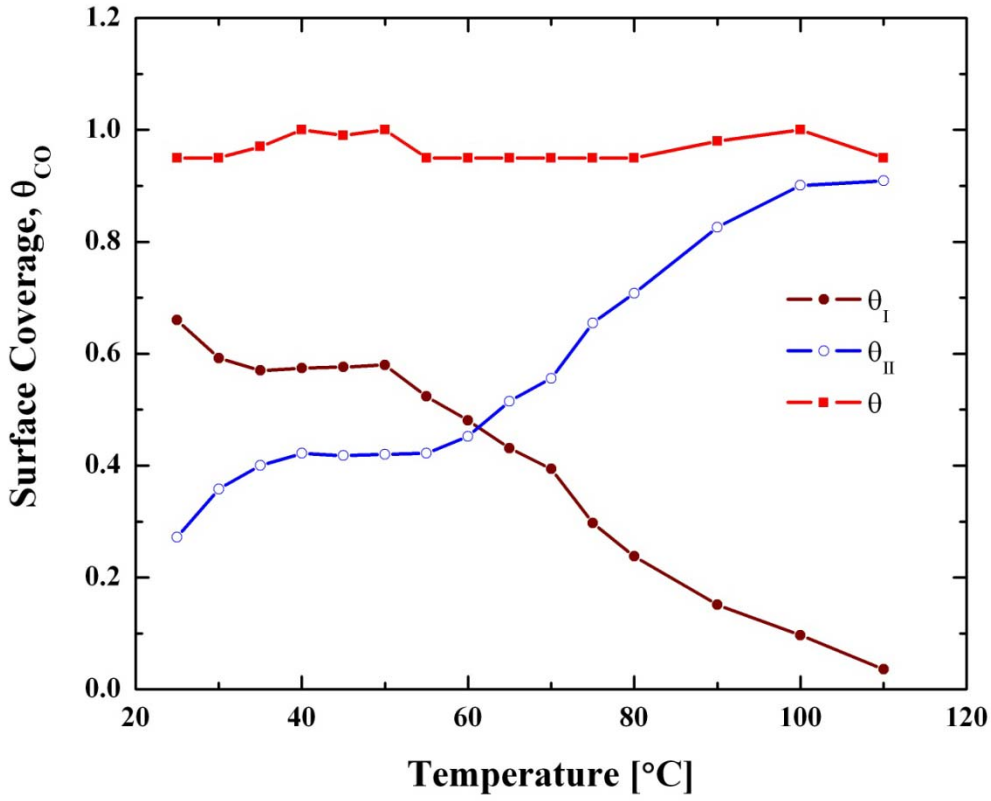

Figure 5: (Color online) Experimentally measured surface coverages of CO_{ad}^{I} (-●-) and CO_{ad}^{II} (-○-) as a function of temperature. These data points were obtained by deconvoluting the CVs from the dataset shown in Figure 4 and using the resulting coulombic charges in equations 2 and 3. The sum of these two coverages (-■-) was 1±0.05.

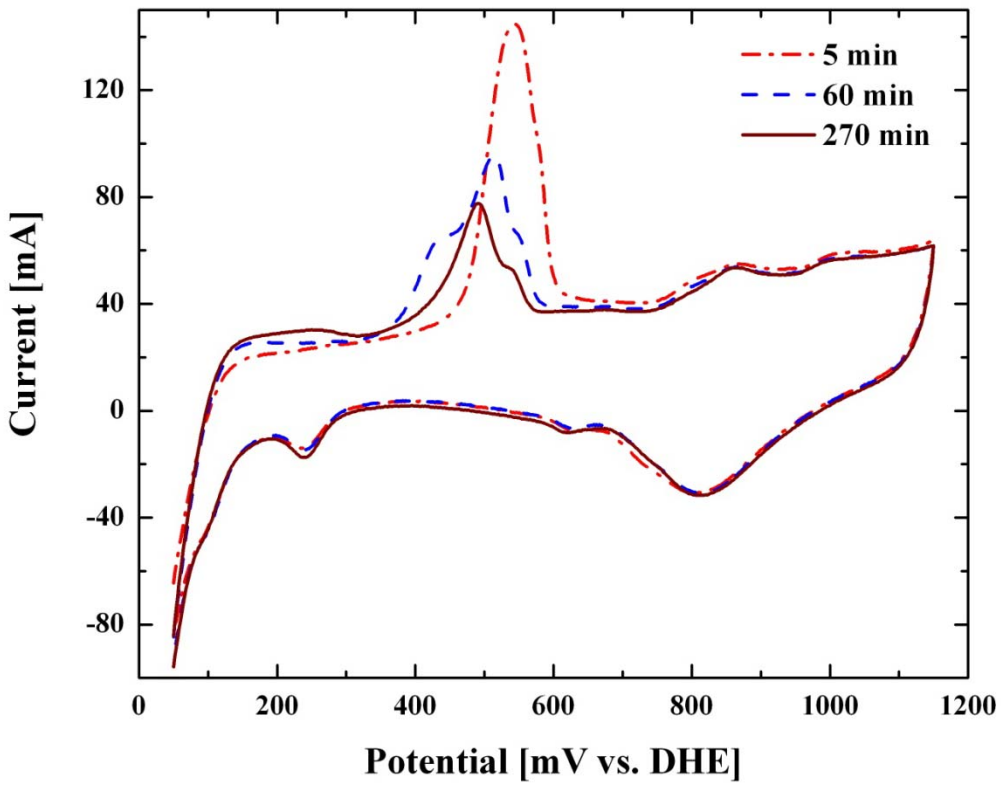

Figure 6: (Color online) CVs on a Pt composite electrode under N_2 flow after three sample desorption times. The electrodes were initially exposed to 476 ppm CO in N_2 for 300 s at 95 °C and 101.325 kPa.

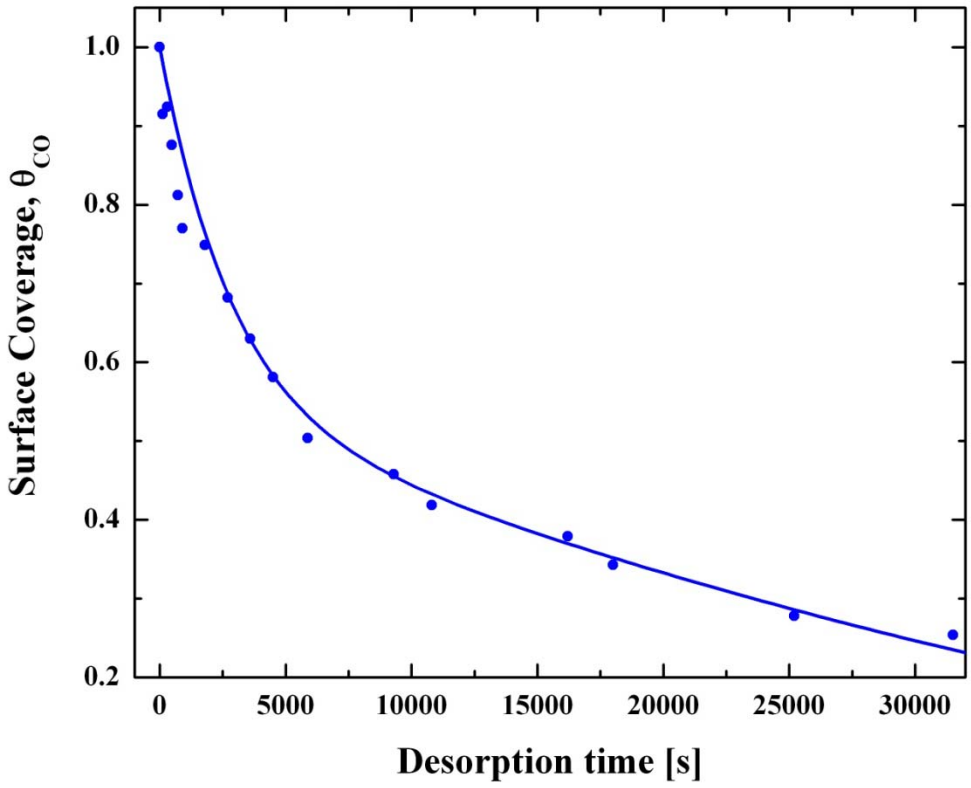

Figure 7: (Color online) Total surface coverage of CO as a function of desorption time at 95 °C and 101.325 kPa. The data (●) was fit (solid line) to the sum of equations 9 and 10.

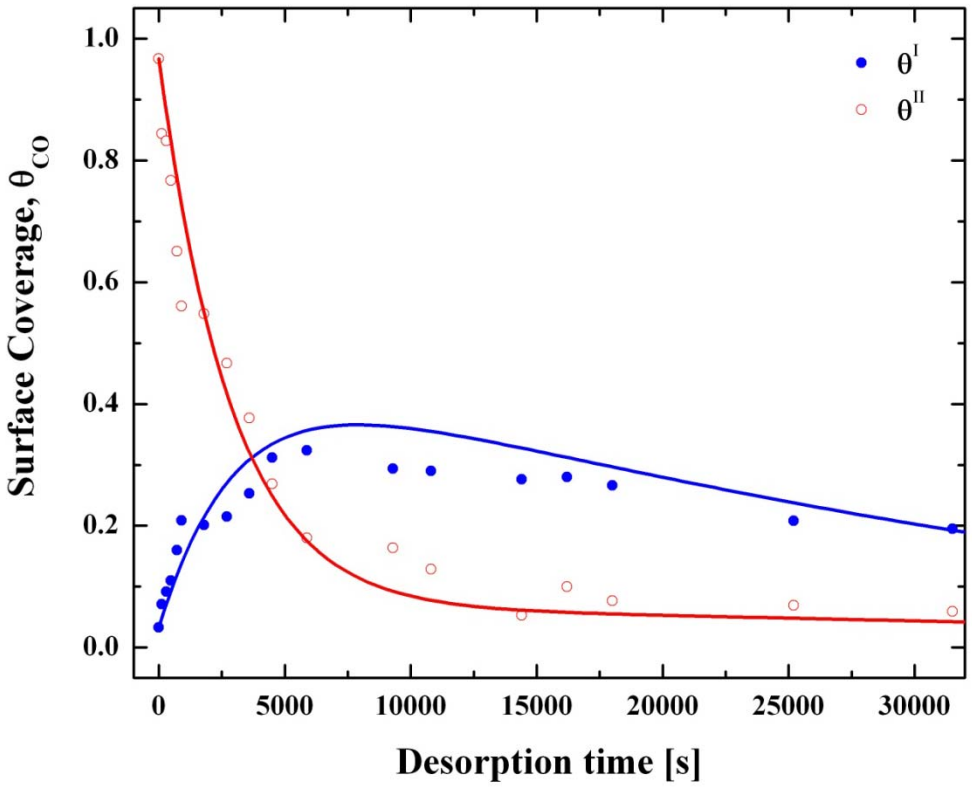

Figure 8: (Color online) Surface coverages of CO_{ad}^{I} (●) and CO_{ad}^{II} (○) molecules measured at 95 °C and 101.325 kPa were compared to model predictions.

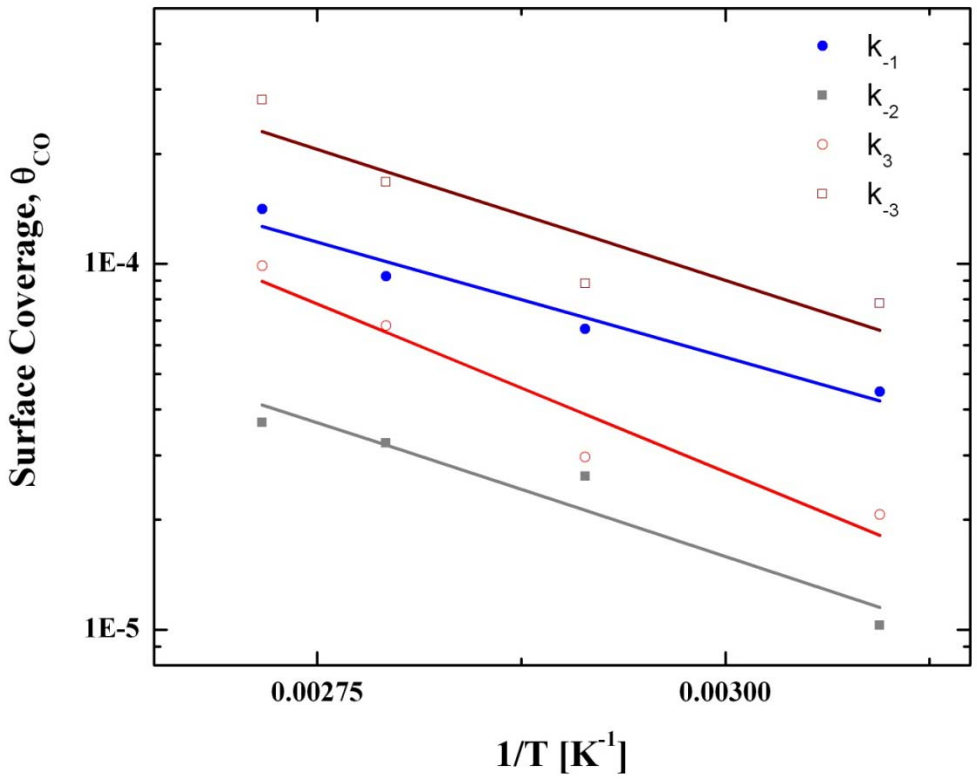

Figure 9: (Color online) Arrhenius plots for desorption (k_{-1}, k_{-2}) and re-arrangement (k_3, k_{-3}) rate constants in the temperature range 50 to 95 °C. The symbols correspond to the different kinetic constants indicated by the legend. The Arrhenius expressions for each of these rate constants are given in equation 12.

References

1. S. Gilman, *J. Phys. Chem.,* **66**, 2657 (1962).

2. S. Gilman, *J. Phys. Chem.*, **67**, 78 (1963).

3. K. Kunimatsu, H. Seki, W. G. Golden, J. G. Gordon II, and M. R. Philpott, *Langmuir,* **2**, 464 (1986).

4. J. Sobkowski, and A. Czerwinski, *J. Phys. Chem.,* **89**, 365 (1985).

5. B. Beden, C. Lamy, N. R. De Tacconi, and A. J. Arvia, *Electrochim. Acta,* **35**, 691 (1990).

6. V. E. Kazarinov, V. N. Andreev, and A. V. Shlepakov, *Electrochim. Acta,* **34**, 905 (1989).

7. A. Cuoto, M. C. Perez, A. Rincon, and C. Gutierrez, *J. Phys. Chem.,* **100**, 19538 (1996).

8. A. Wieckowski, M. Rubel, and C. Gutierrez, *J. Electroanal. Chem.,* **382**, 97 (1995).

9. R. D. Eischens and W. Pliskin, Advances in Catalysis, Vol. X, Academic Press, Inc., New York, N. Y., 1958, p. 18

10. S-C. Chang, and M. J. Weaver, *J. Phys. Chem.,* **94**, 5095 (1990).

11. F. Kitamura, M. Takahashi, and M. Ito, *Surf. Science*, **223**, 493 (1989).

12. I. Villegas, and M. J. Weaver, *J. Chem. Phys.,* **101**, 1648 (1994).

13. H. Kita, H. Naohara, T. Nakato, S. Taguchi, and A. Aramata, *J. Electroanal. Chem.,* **386**, 197 (1995).

14. N. M. Markovic, B. N. Grgur, C. A. Lucas, and P. N. Ross, *J. Phys. Chem. B.,* **103**, 487 (1999).

15. E. Pastor, J. L. Rodriguez, and T. Iwasita, *Electrochem. Comm.*, **4**, 959 (2002).

16. A. Constantinides and N. Mostoufi, *Numerical Methods for Chemical Engineers with MATLAB Applications*, pp. 439-481, Prentice Hall, Upper Saddle River, NJ (1999).

17. B. Lakshmanan, W. Huang and J. W. Weidner, *Electrochem. Sol. State Let.*, **5**, A267 (2002).